

Electronic Supporting Information

***In-situ* luminescence analysis: a new light on monitoring calcium phosphate phase transitions**

Huayna Terraschke,^{a,*} Merrit Rothe,^a Anna-Maria Tsigirigi,^a Patric Lindenberg,^a
Laura Ruiz Arana,^a Niclas Heidenreich,^{a, b} Florian Bertram,^b Martin Etter^b

^a Institut für Anorganische Chemie, Christian-Albrechts-Universität zu Kiel,
Max-Eyth-Str. 2, 24118 Kiel, Germany. E-mail: hterraschke@ac.uni-kiel.de

^b DESY Photon Science, Notkestr. 85, 22607 Hamburg, Germany.

Contents

1. Experimental section	2
1.1. Setup A at the University of Kiel	2
1.2. Setup B at DESY	4
2. Influence of doping concentration	6
3. Influence of the type of coordination sensor	8
4. Influence of the reactants concentration	9
5. <i>In-situ</i> excitation spectra of Ce ³⁺ -doped calcium phosphate	14
6. Supplementary <i>in-situ</i> infrared spectra	16
7. Experiments at the Deutsches Elektronen-Synchrotron DESY	17
7.1. Eu ³⁺ -doped calcium phosphate	17
7.2. Ce ³⁺ -doped calcium phosphate	19
8. References	21

1. Experimental section

1.1. Setup A at the University of Kiel

Experiments at the University of Kiel have been performed applying a stationary EasyMax[®] 102 (Mettler Toledo, Gießen, Germany) synthesis workstation, with integrated automatic dosing system, stirring unit and temperature control. This setup is important for the strict control of the synthesis parameters. Since the nucleation, crystal growth and phase transitions of calcium phosphate are very sensitive to the synthesis conditions and suffer a strong influence from e.g. stirring and flow rate, these parameters must be kept constant for every experiment. ^[1] The reactions are carried out in a glass reactor, which cover comprises several openings for the integrated sensors for *in-situ* measuring pH, conductivity and attenuated total reflectance Fourier transform infrared (ATR-FT-IR) spectroscopy (Mettler Toledo, Gießen, Germany, Fig. S1). The recorded *in-situ* IR data has been analyzed with aid of the *In-situ* IR Data Helper ^[2] software. *In-situ* Luminescence measurements were performed applying a FL3-22 Fluorolog-3 fluorescence spectrometer (HORIBA Jobin Yvon GmbH, Unterhaching, Germany), containing a Sincerity charge-coupled device (CCD) detector, a R928P Photomultiplier, a 450 W xenon lamp and an iHR-320-FA triple grating imaging spectrograph. The spectrometer was connected to the reactor by means of a Y-shaped optical fibre, which transported the excitation light from the spectrometer to the sample and the emitted light from the sample to the detector. *In-situ* luminescence spectra have been recorded every 30 s.



Figure S1. Combination of the ILACS technique with *in-situ* pH, conductivity and infrared spectroscopy measurements.

Since undoped calcium phosphate species are not optical active, the *in-situ* luminescence analysis of coordination sensors (ILACS) ^[3] approach was used for monitoring the respective

transitions by recording *in-situ* luminescence spectra. This approach profits from the sensitivity of lanthanide ions as Eu^{3+} , Ce^{3+} or Tb^{3+} to the coordination environment, using them as local coordination sensors. Thus, these ions are incorporated by the investigated material during synthesis, and local changes around the cation sites caused by e.g. the formation of the solid materials or phases transitions are detected measuring *in-situ* luminescence spectra under real reaction conditions (Fig. S2). This method consists of a valuable complementation to *in-situ* X-ray diffraction (XRD) analysis, because it does not depend on synchrotron radiation and can be flexibly carried out at conventional university laboratories.

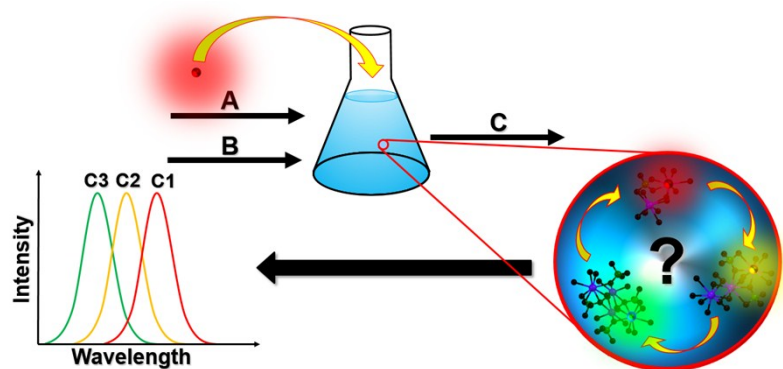


Figure S2. Principle of the ILACS technique: lanthanide ions incorporated as local sensor by the investigated material. Changes in the coordination environment of the cations sites are detected by *in-situ* luminescence measurements recorded under real reaction conditions.

For the application of *ex-situ* characterization techniques, 1 mL samples have been removed from the reactor after fixed time intervals, quenched, centrifuged, washed with water and ethanol and dried at 80 °C for 2 h. *Ex-situ* XRD measurements were performed in transmission geometry applying a STOE Stadi-p X-ray powder diffractometer (STOE & Cie GmbH, Darmstadt, Germany) with a DECTRIS® MYTHEN 1K detector (DECTRIS, Baden-Daettwil, Switzerland) with Cu $\text{K}\alpha_1$ radiation ($\lambda = 1.54056 \text{ \AA}$) and Ge monochromator. A Philips Environmental Scanning Electron Microscope ESEM XL30 was used for recording the *ex-situ* microscope images.

1.2. Setup B at DESY

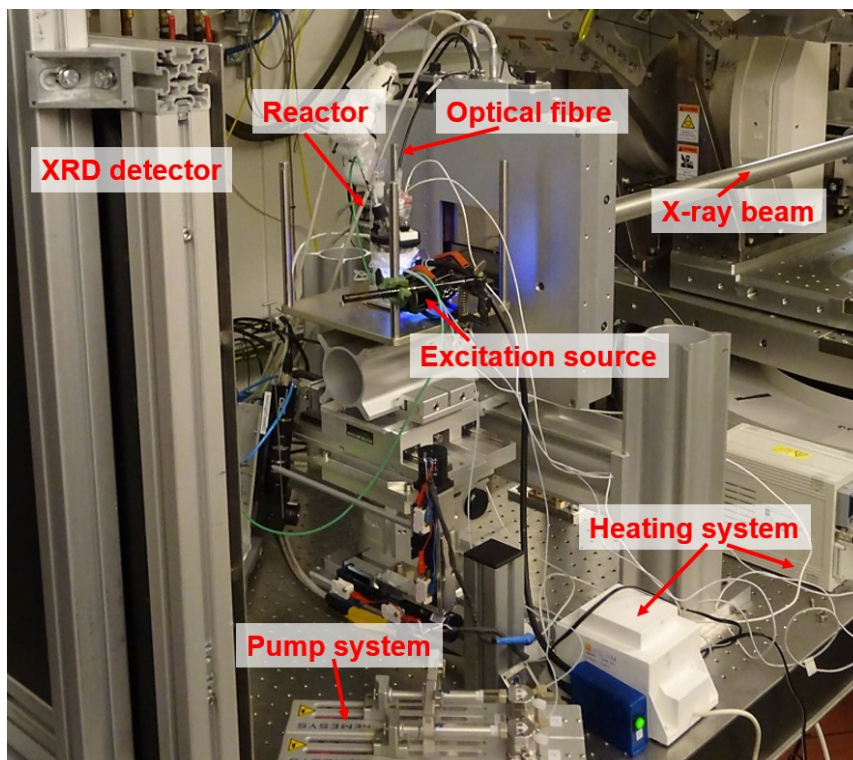


Figure S3. Setup at the PETRA III beamline P08, showing the pathway of the X-ray beam, XRD detector, reactor, pump and heating systems as well as optical fiber and excitation source for *in-situ* luminescence measurements (experiment 9, Table 1).

The *in-situ* XRD measurements discussed in this work were performed at the PETRA III Beamlines P08 ^[4] and P02.1 ^[5] at the Deutsches Elektronen-Synchrotron (DESY) in Hamburg, Germany. The high energy and high flux of the synchrotron X-rays are necessary for penetrating the reactor glass walls and the solution bulk volume. At both beamlines, a Perkin Elmer XRD1621 detector (PerkinElmer Technologies, Walluf, Germany) (2048 × 2048 pixels, X pixel size 200.00 μm, Y pixel size 200.00 μm) was applied, recording powder diffraction patterns every 30 s. Measurements at P08 were carried out with energy of 25 keV ($\lambda = 0.4959 \text{ \AA}$) and detector distance of 550 mm, while measurements at P02.1 were performed with energy of 60 keV ($\lambda = 0.20760 \text{ \AA}$) and detector distance of 1060 mm. Figure S3 shows the *in-situ* setup used for the experiments at the P08 beamline, including a reactor holder, designed to flexibly fit different beamlines, the 365 nm excitation source (Sahlmann Photochemical Solutions, Germany), the optical fibre submersed in the reactor content, which transports the emitted light from the reactor to a portable EPP2000 (StellarNet Inc., United States) spectrometer, equipped with a ccd-based detector. During the reactions, the temperature could be raised applying heating wires, connected to a control system (LR 316

laboratory temperature control unit, JUMO GmbH & Co. KG), which was switched on and off via wireless local area network (WLAN) by a mobile phone from outside the measurement hutch. An automatic pump system (neMESYS Syringe Pump, Cetoni GmbH) enabled the addition of the solutions to the reactor.

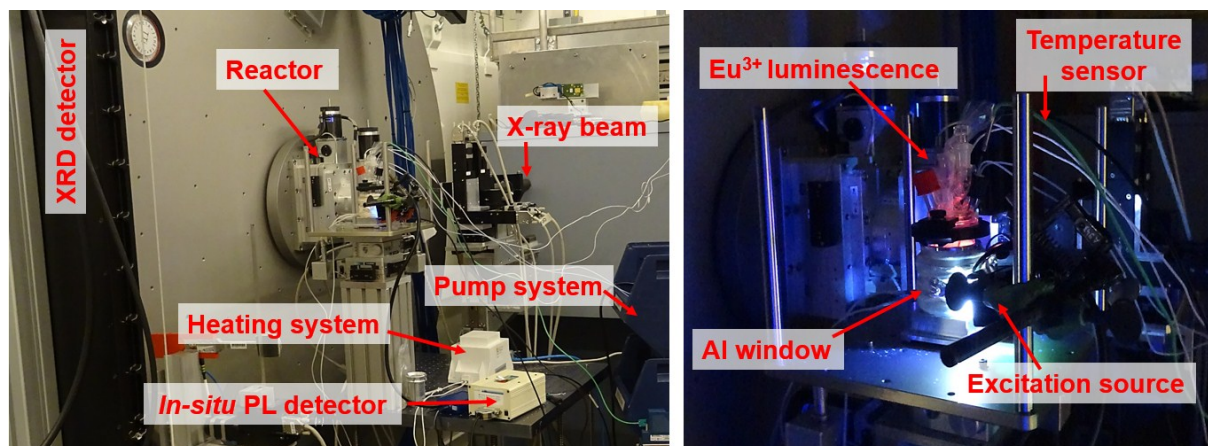


Figure S4. Setup at the PETRA III beamline P02.1, showing the pathway of the X-ray beam, XRD detector, reactor, pump and heating systems, besides photoluminescence (PL) detector (left, experiment **10**, Table 1). Reactor holder showing red luminescence of Eu³⁺-doped calcium phosphate (experiment **10**, Table 1), when irradiated with 365 nm excitation source, temperature sensor and aluminum window, used for normalizing the intensity of the *in-situ* XRD patterns.

Figure S4 shows a similar setup for the experiments performed at the P02.1 beamline, with an additional enlargement of the reactor holder, highlighting the use of an aluminum window. This aluminum window functions as an external standard for normalizing the intensities of the XRD patterns, attenuating the effect of intensity fluctuation of the X-ray beam.^[6] All DESY data have been analyzed with aid of the Fit2D,^[7] DESY data helper^[2] and *in-situ* luminescence data helper^[2] computer programs. The same 365 nm light source and portable spectrometer described for the experiments carried out at P08 (experiment **9**, Table 1), was used at the P02.1 beamline for measuring the time dependence of the light transmission and turbidity during synthesis of Ce³⁺-doped calcium phosphate (experiment **10**, Table 1), which is not luminescent upon excitation with this wavelength. As explained in our previous work,^[8] this approach is advantageous for *in-situ* monitoring the formation of solid materials due to its simplicity and because it does not depend on the wavelength of the light source or if the analysed material is luminescent or not, increasing its applicability. Hence, the reactor is illuminated by the light source from outside the reactor, while the optical fiber submerged in the reactor content measures the changes of the intensity of the light source through the

mother solution during the reaction. Upon the formation of solid material, the turbidity of the solution increases, blocking the passage of the light source, decreasing its intensity.

2. Influence of doping concentration

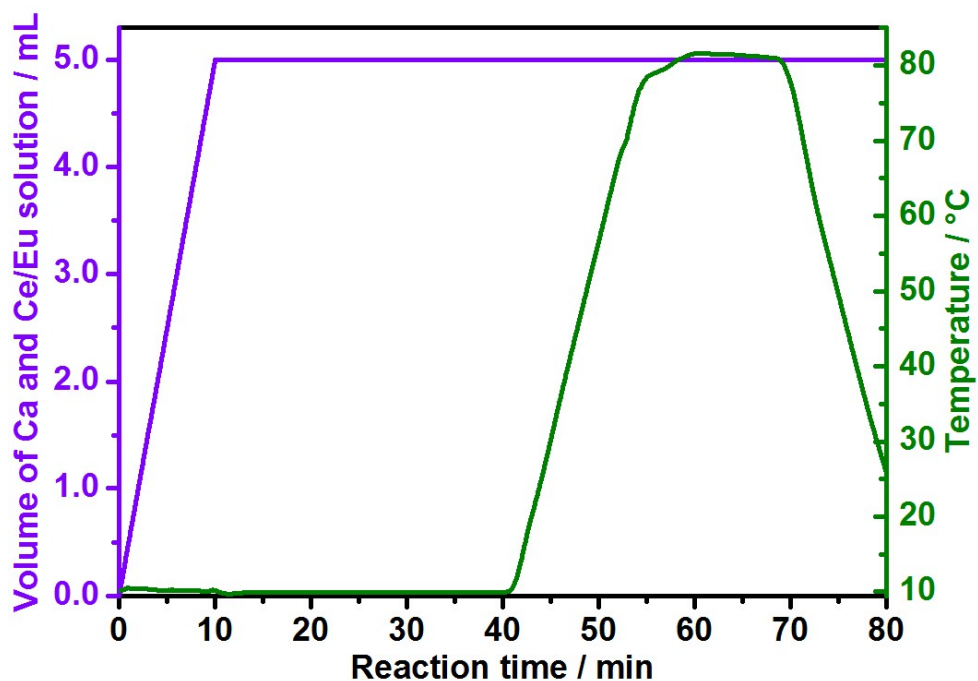


Figure S5. General experiment program including the time-dependence of the temperature and of the addition of the solution of calcium and cerium or europium nitrates to the reactor containing diammonium hydrogenphosphate, used on experiments displayed on Figures 1-4 and Figures S6-S7 (experiments 1-7, Table 1).

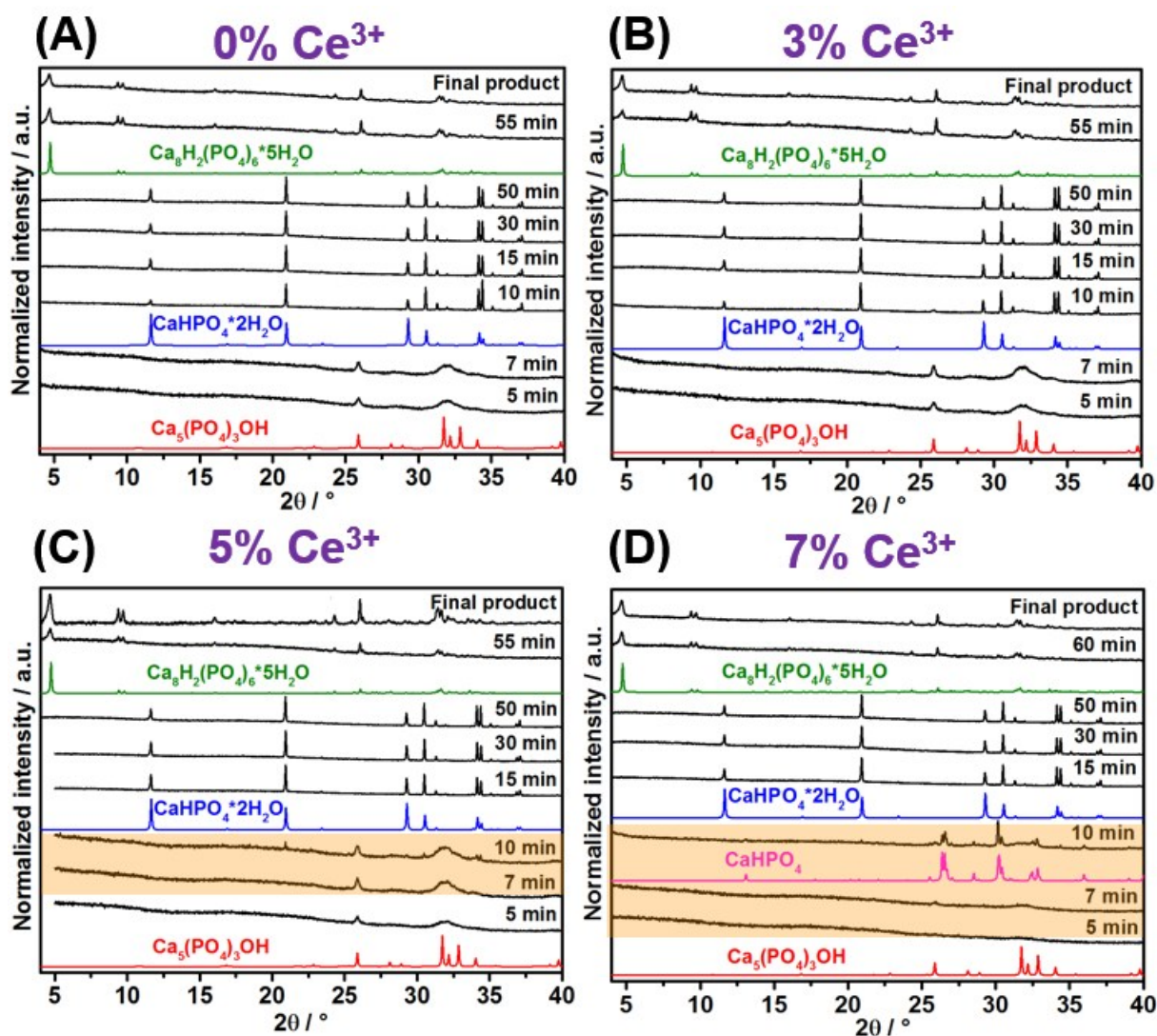


Figure S6. *Ex-situ* XRD measurements of samples removed during synthesis of calcium phosphate for a) 0% (experiment 1, Table 1), b) 3% (experiment 2, Table 1), c) 5% (experiment 4, Table 1) and d) 7% (experiment 5, Table 1) of doping concentration, in comparison to calculated diffraction patterns of $\text{Ca}_5(\text{PO}_4)_3\text{OH}$, $^{[9]}$ $\text{CaHPO}_4 \cdot 2\text{H}_2\text{O}$ $^{[10]}$ and $\text{Ca}_8(\text{HPO}_4)_2(\text{PO}_4)_4 \cdot 5\text{H}_2\text{O}$ $^{[11]}$.

3. Influence of the type of coordination sensor

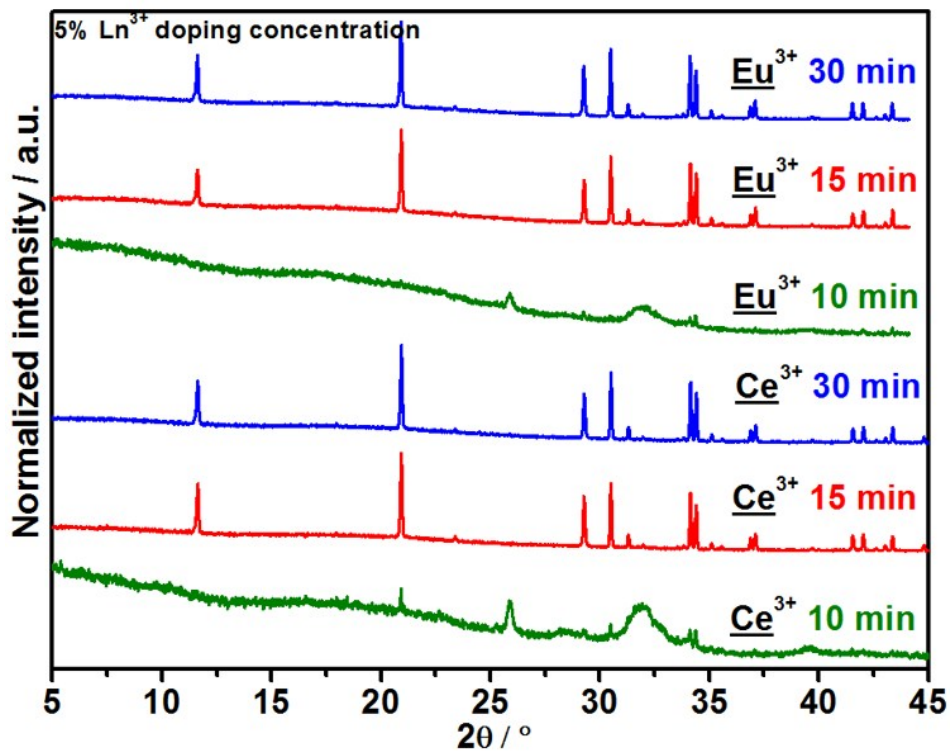


Figure S7. Comparison of *ex-situ* XRD analysis of samples removed at $t = 10$ min (green curve), $t = 15$ min (red curve) and $t = 30$ min (blue curve) during the calcium phosphate synthesis doped with 5% Ce^{3+} (experiment 4, Table 1) and 5% Eu^{3+} (experiment 7, Table 1). The similarity of these diffraction patterns demonstrates that the type of coordination sensor does not significantly influence the transitions among the calcium phosphate phases.

4. Influence of the reactants concentration

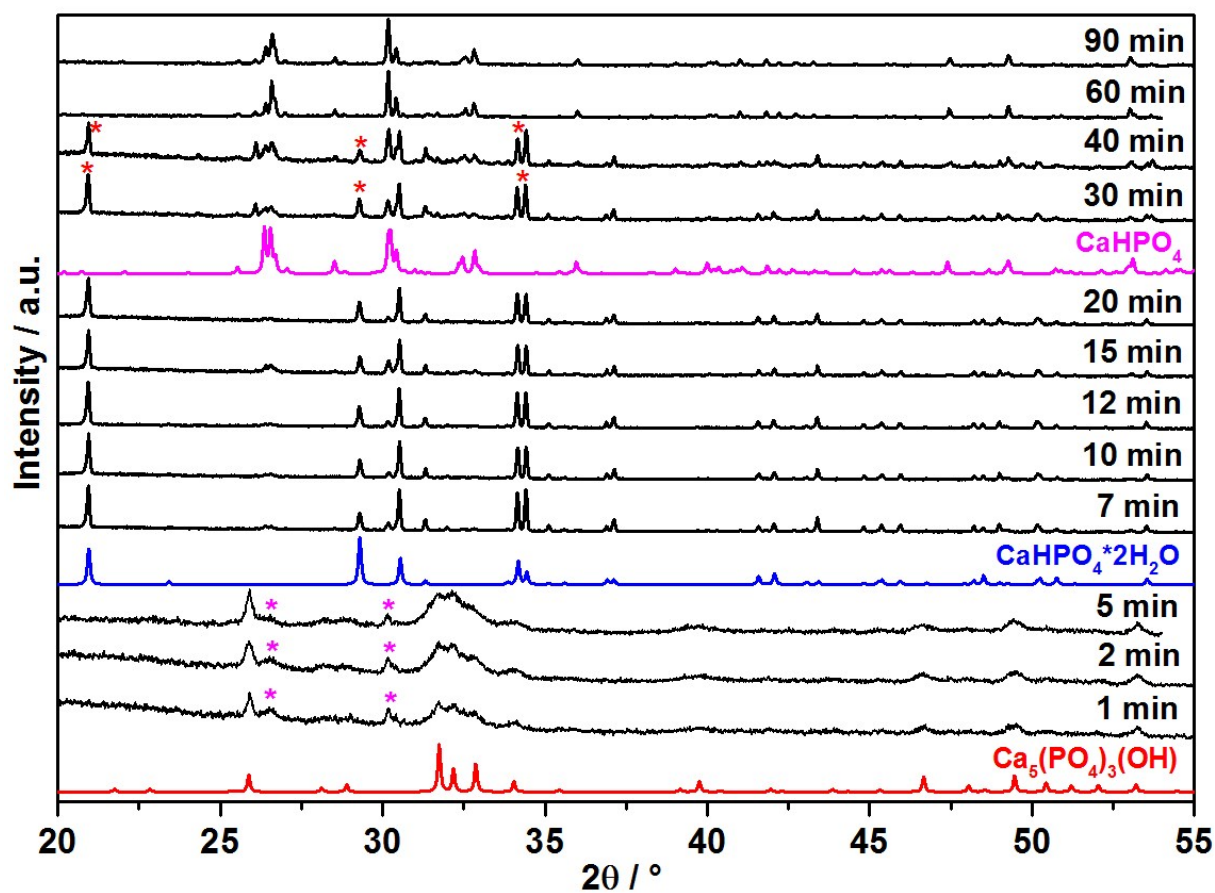


Figure S8. *Ex-situ* XRD analysis of samples removed during synthesis of europium-doped calcium phosphate for reactant concentration (experiment **8**, Table 1) 3.3 times higher than experiments **4** and **7** (Table 1). As shown in detail on Fig. S7, the elevation of the temperature to 80 °C at $t > 20$ min causes the transition from $\text{CaHPO}_4 \cdot 2\text{H}_2\text{O}$ ^[10] to CaHPO_4 ,^[12] instead of the transition to $\text{Ca}_8(\text{HPO}_4)_2(\text{PO}_4)_4 \cdot 5\text{H}_2\text{O}$ ^[11] observed on Fig. S6c for experiments **4** (Table 1).

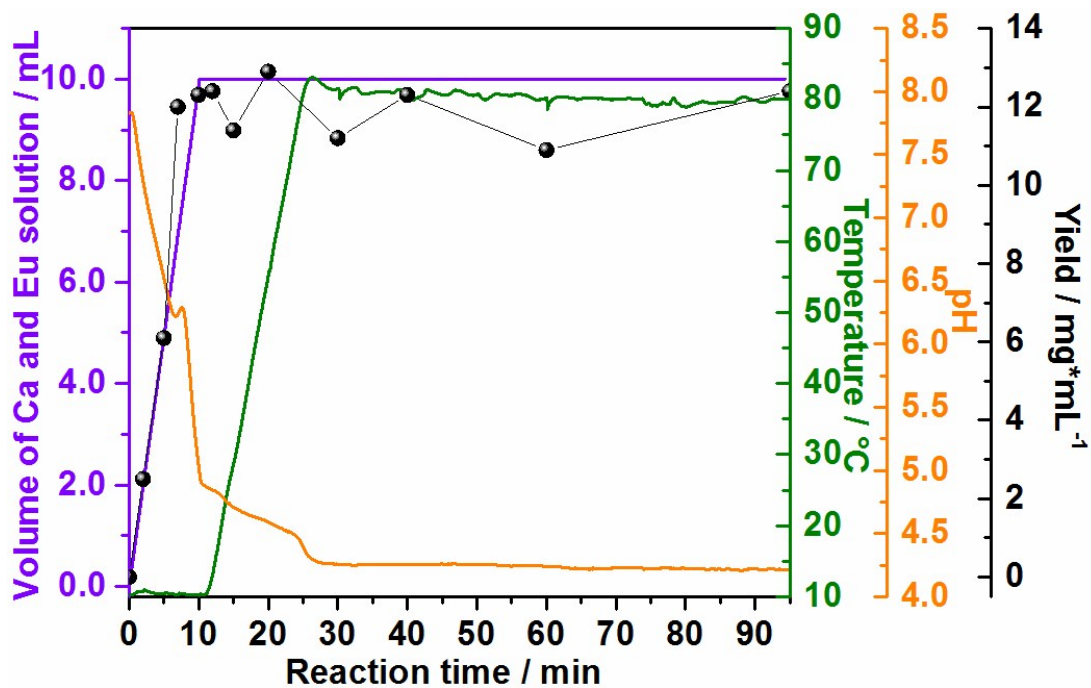


Figure S9. Dependence of the product concentration (black spheres) and pH (orange curve) on the temperature (green curve) and addition of the calcium and europium solution (violet curve) to the reactor containing $(\text{NH}_4)_2\text{HPO}_4$ solution (experiment 8, Table 1).

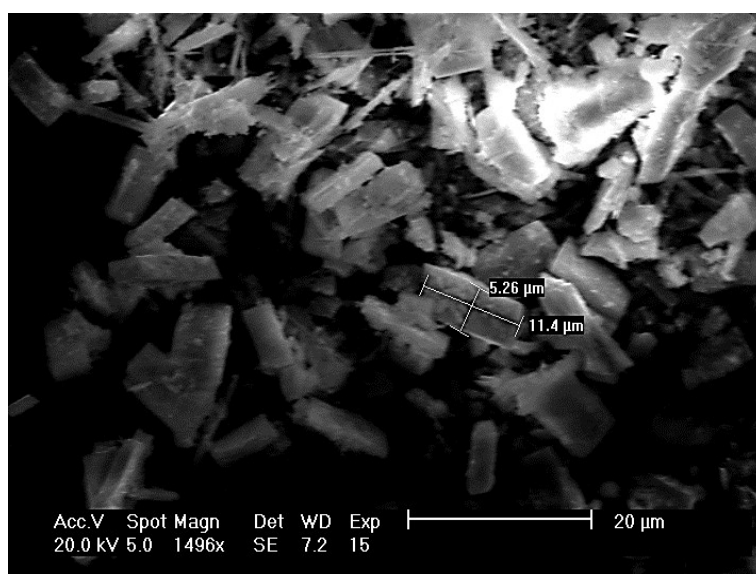
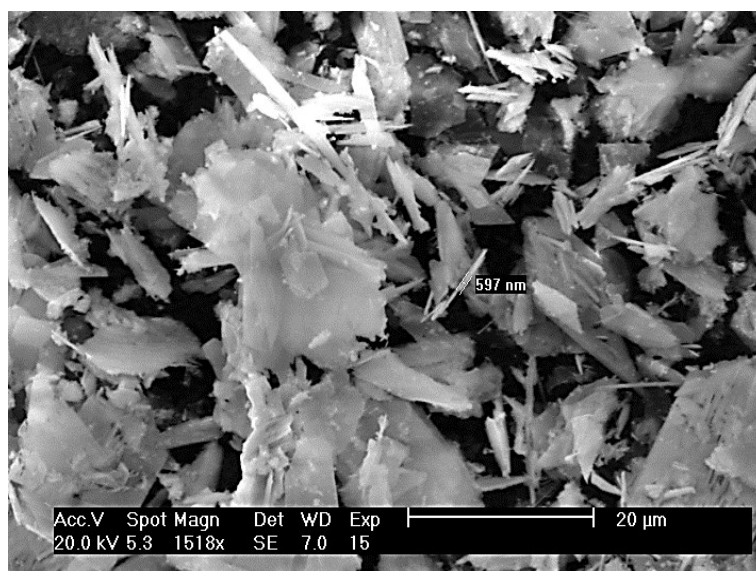
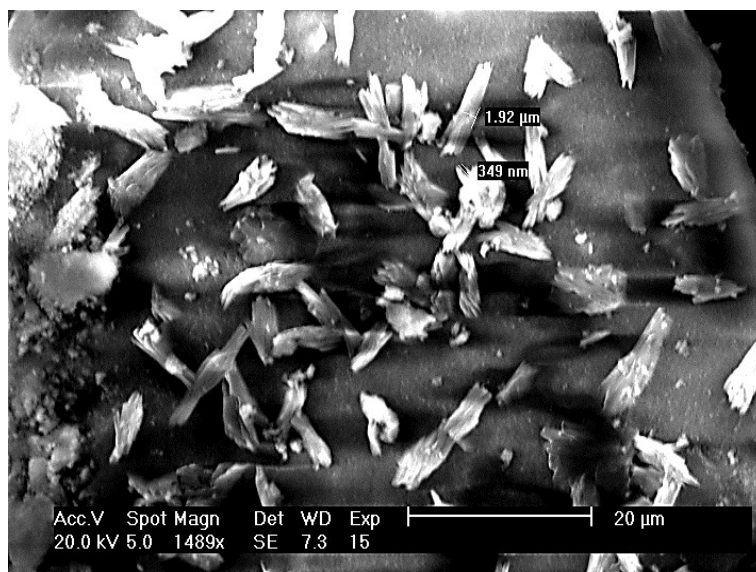


Figure S10. Scanning electron images of samples removed from the reactor 1 min (top), 20 min (middle), 60 min (bottom) during synthesis of calcium phosphate (experiment 8, Table 1).

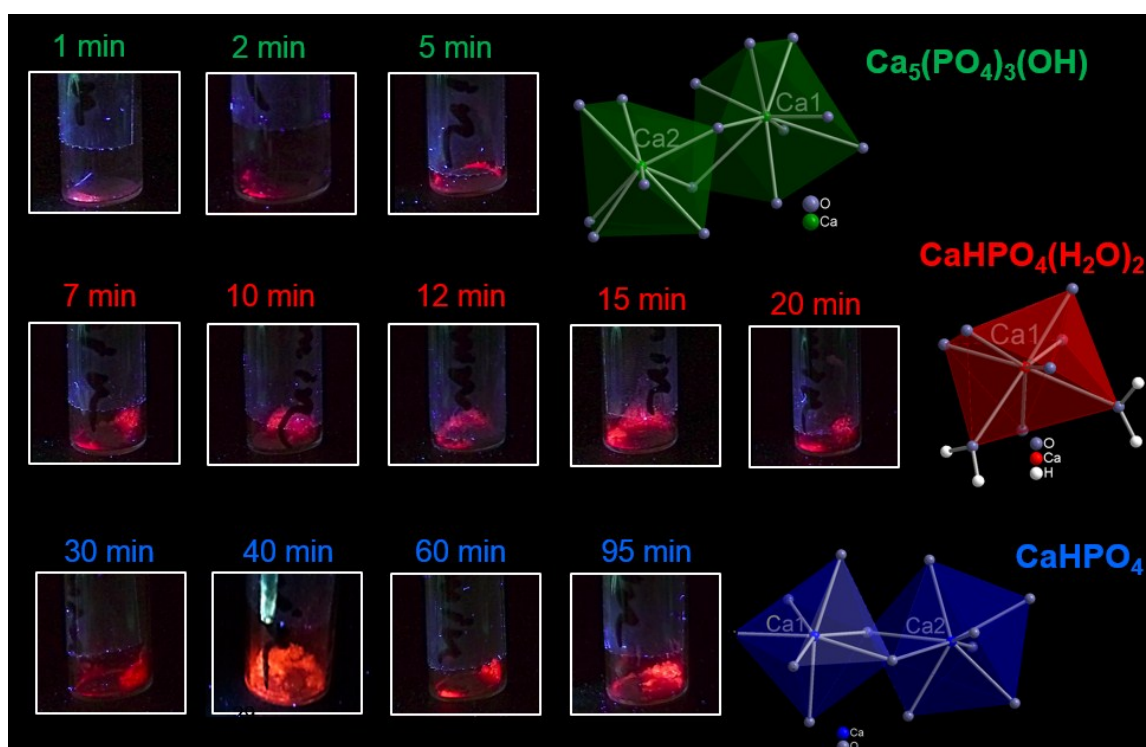


Figure S11. Irradiation with UV light of samples removed from the reactor during the synthesis of Eu^{3+} -doped calcium phosphate at $t = 1\text{-}5$ min, $t = 7\text{-}20$ min and $t = 30\text{-}95$ min, assigned to $\text{Ca}_5(\text{PO}_4)_3(\text{OH})$,^[9] $\text{CaHPO}_4 \cdot 2\text{H}_2\text{O}$ ^[10] and CaHPO_4 ,^[11] respectively (experiment 8, Table 1).

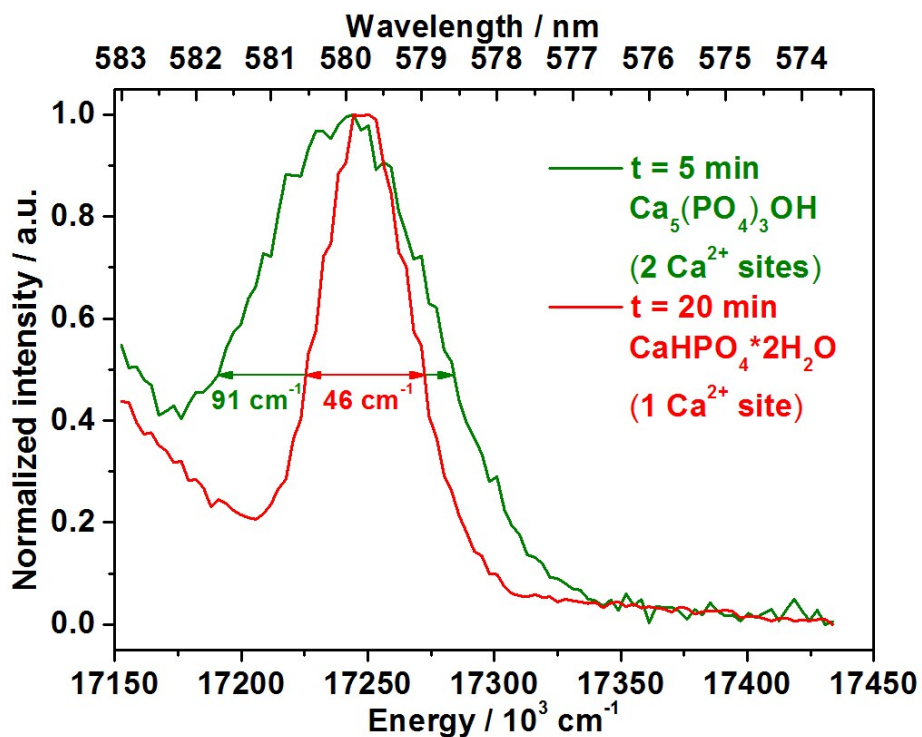


Figure S12. Comparison between full width at half maximum (fwhm) of ${}^5D_0 \rightarrow {}^7F_0$ transition for $\text{Ca}_5(\text{PO}_4)_3\text{OH}$ (2 cations sites, green curve) ^[9] and $\text{CaHPO}_4 \cdot 2\text{H}_2\text{O}$ (1 cation site, red curve) ^[10] for samples removed from the reactor at $t = 5$ min and $t = 20$ min during synthesis of calcium phosphate (experiment 8, Table 1).

5. *In-situ* excitation spectra of Ce³⁺-doped calcium phosphate

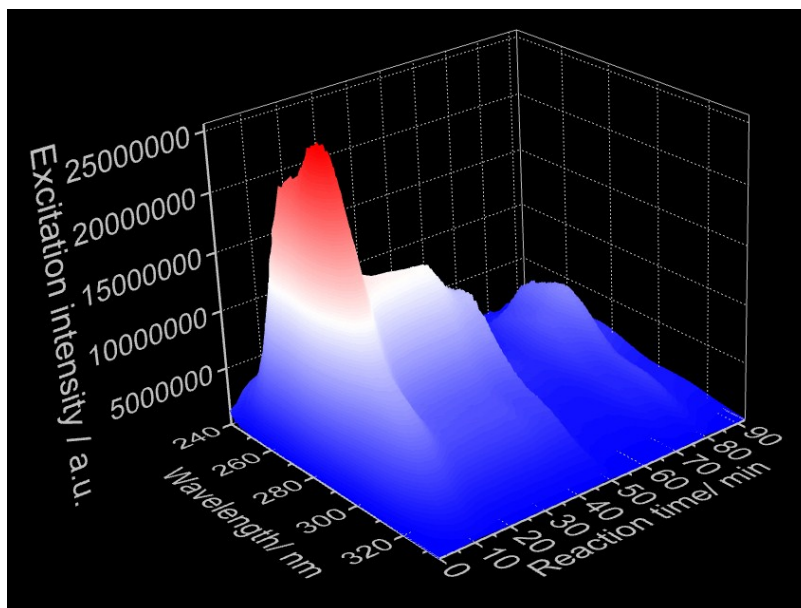


Figure S13. *In-situ* excitation spectra recorded during calcium phosphate phase transitions applying 3% Ce³⁺ as coordination sensor ($\lambda_{em} = 365$ nm, experiment 3, Table 1).

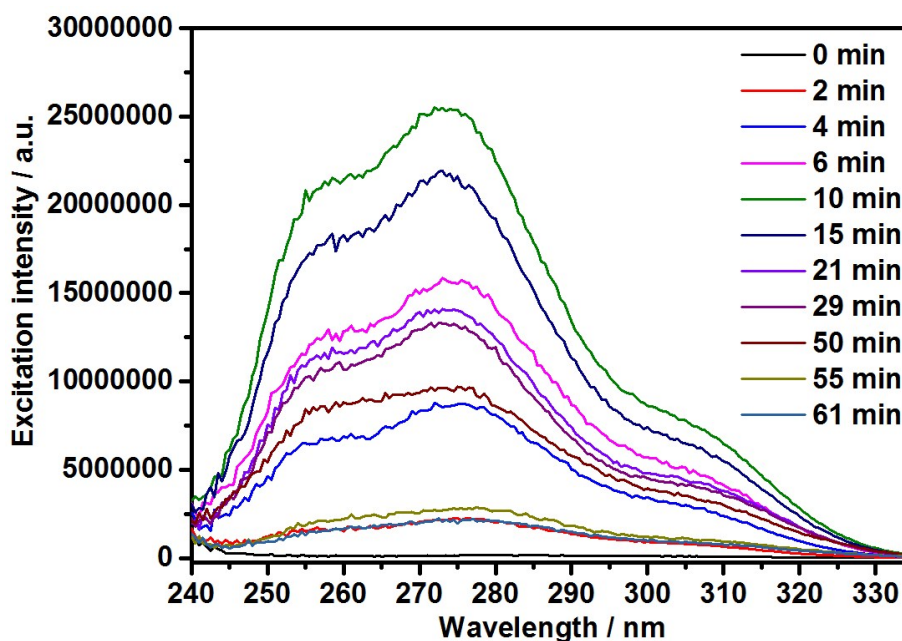


Figure S14. 2D plot for *in-situ* excitation spectra recorded during calcium phosphate phase transitions applying 3% Ce³⁺ as coordination sensor ($\lambda_{em} = 365$ nm, experiment 3, Table 1).

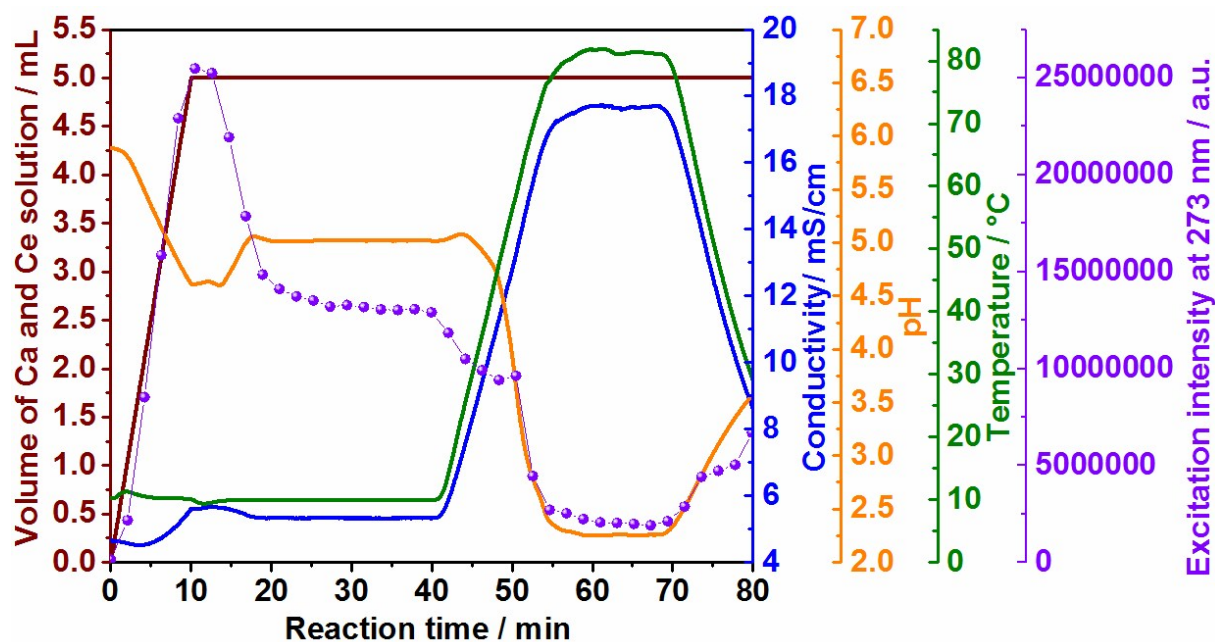


Figure S15. Time dependence of the excitation intensity of Ce^{3+} ($\lambda_{\text{em}} = 365 \text{ nm}$, violet curve) doped calcium phosphate, *in-situ* ion conductivity (blue curve) and *in-situ* pH (orange curve) in comparison the volume of the Ca^{2+} and Ce^{3+} solution (brown curve) to the reactor containing aqueous $(\text{NH}_4)_2\text{HPO}_4$ (experiments 3, Table 1).

6. Supplementary *in-situ* infrared spectra

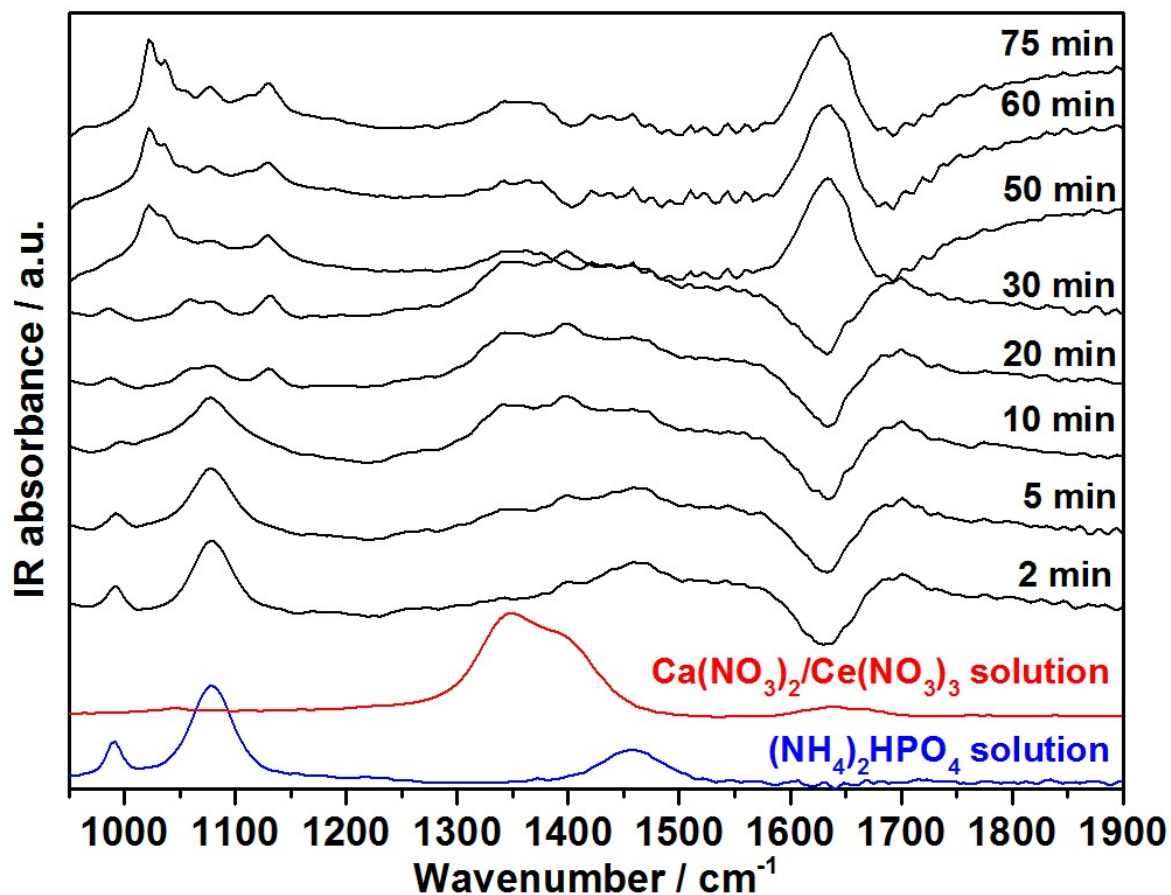


Figure S16. Comparison of *in-situ* IR spectra of the reactants solutions of calcium and cerium nitrate (red curve) as well as diammonium hydrogen phosphate (blue curve) with selected reaction times ($t = 2, 5, 10, 20, 30, 50, 60$ and 75 min) during the synthesis of cerium-doped calcium phosphate (experiment 2, Table 1).

7. Experiments at the Deutsches Elektronen-Synchrotron DESY

7.1. Eu^{3+} -doped calcium phosphate

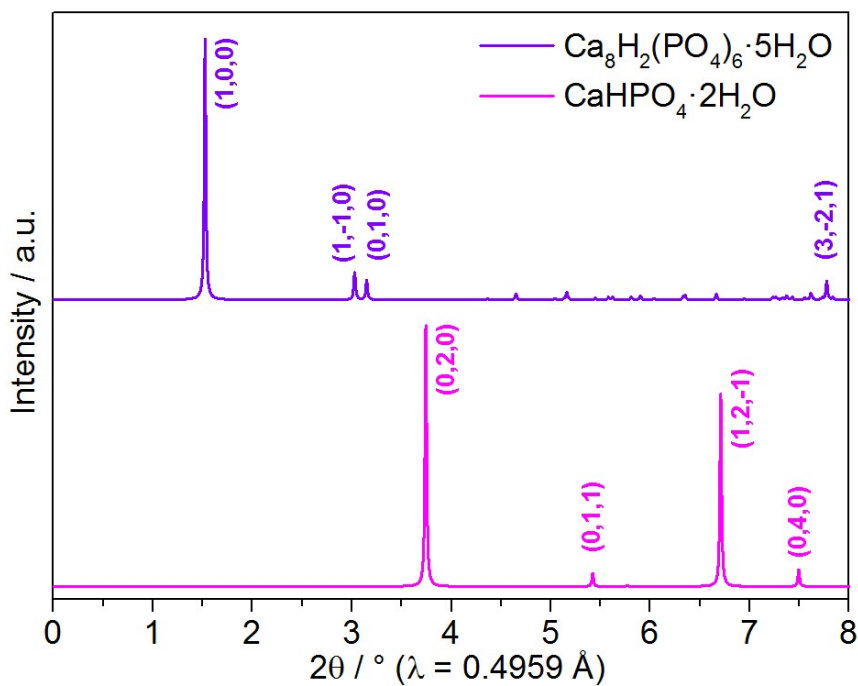


Figure S17. Calculated XRD patterns ($\lambda = 0.4959 \text{ \AA}$, 25 keV) of $\text{CaHPO}_4 \cdot 2\text{H}_2\text{O}$ ^[10] (pink curve) and $\text{Ca}_8\text{H}_2(\text{PO}_4)_6 \cdot 5\text{H}_2\text{O}$ ^[11] (violet curve) for assigning respective reflections on *in-situ* XRD measurements of Fig. S18, recorded at the DESY P08 beamline.

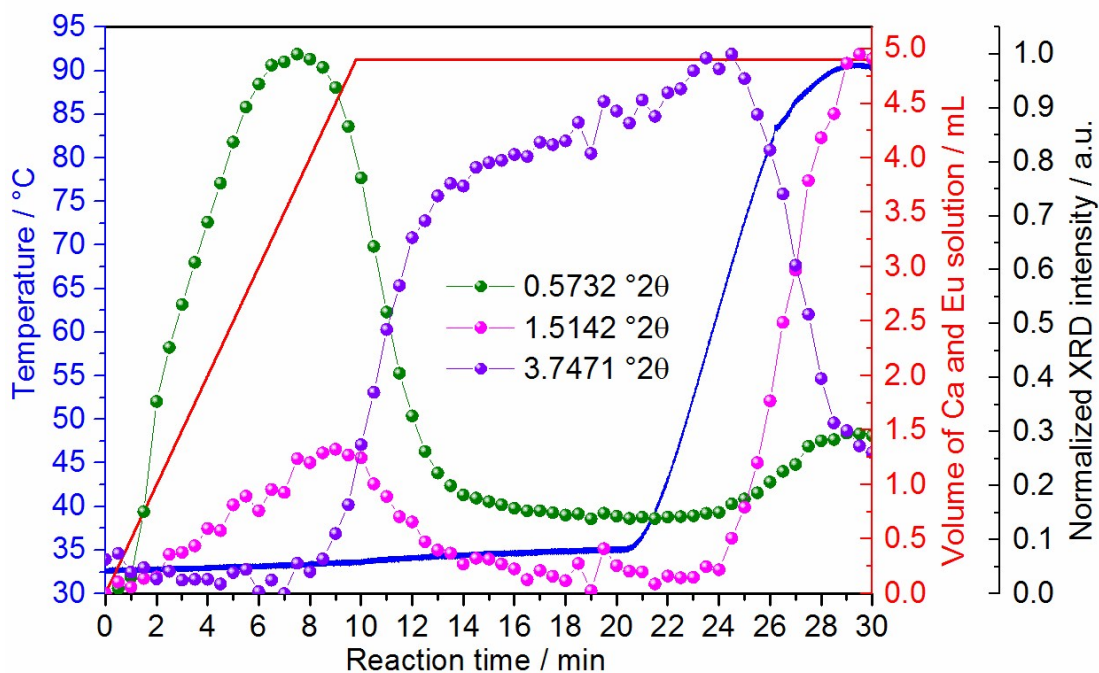


Figure S18. Normalized intensity of XRD reflections ($\lambda = 0.4959 \text{ \AA}$) at $0.5732^\circ 2\theta$ (green curve, assigned to the amorphous phase ^[13]), $1.5142^\circ 2\theta$ (pink curve, (1,0,0) reflection of $\text{Ca}_8\text{H}_2(\text{PO}_4)_6 \cdot 5\text{H}_2\text{O}$, ^[11] Fig. S24) and $3.7471^\circ 2\theta$ (violet curve, (0,2,0) reflection of $\text{CaHPO}_4 \cdot 2\text{H}_2\text{O}$, ^[10] Fig. S18), measured at the DESY P08 beamline (experiment **9**, Table S1).

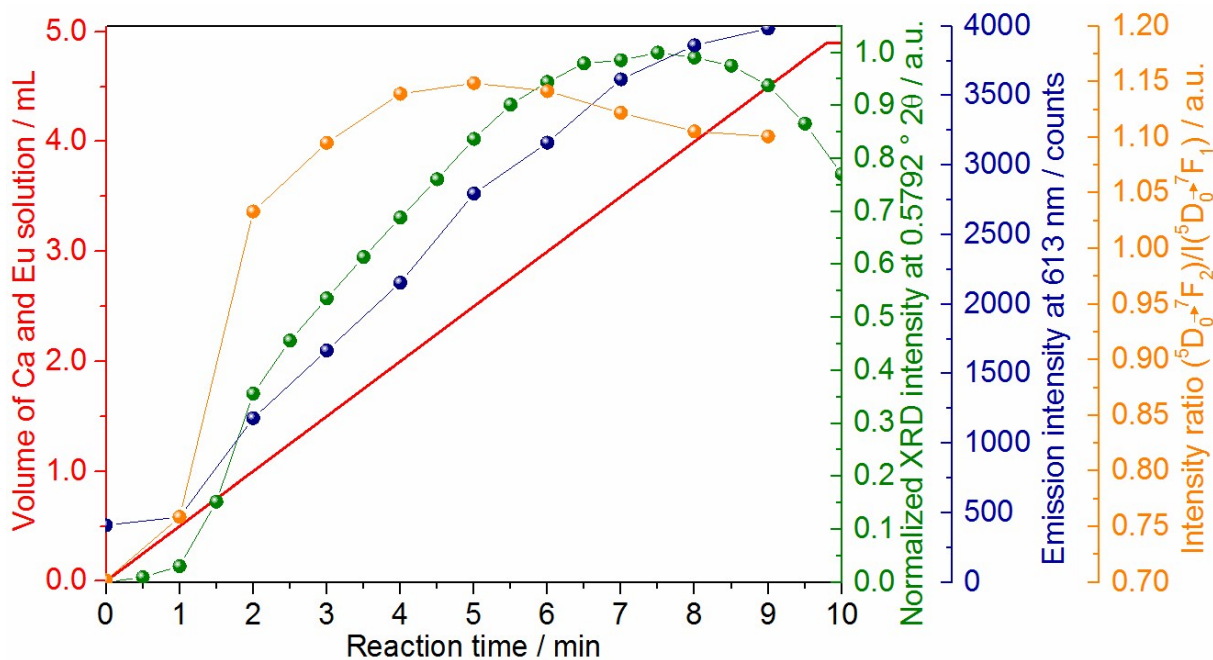


Figure S19. Comparison of normalized intensity of XRD reflections at $0.5732^\circ 2\theta$ (green curve, assigned to the amorphous phase ^[13]) to the volume of Ca and Eu solution, emission intensity at 613 nm and intensity ratio between $\text{Eu}^{3+} \ ^5\text{D}_0 \rightarrow \ ^7\text{F}_2$ and $\ ^5\text{D}_0 \rightarrow \ ^7\text{F}_1$ transitions (experiment 9, Table 1).

7.2. Ce^{3+} -doped calcium phosphate

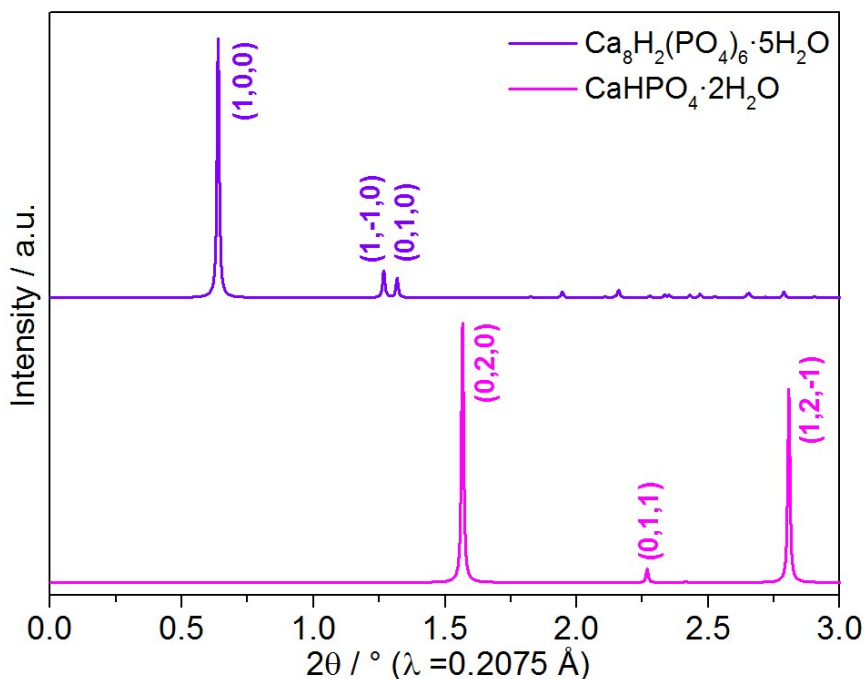


Figure S20. Calculated XRD patterns ($\lambda = 0.2075 \text{ \AA}$, 60 keV) of $\text{CaHPO}_4 \cdot 2\text{H}_2\text{O}$ ^[10] (pink curve) and $\text{Ca}_8\text{H}_2(\text{PO}_4)_6 \cdot 5\text{H}_2\text{O}$ ^[11] (violet curve) for assigning respective reflections on *in-situ* XRD measurements of Fig. 5 and Fig. S22, recorded at the DESY P02.1 beamline.

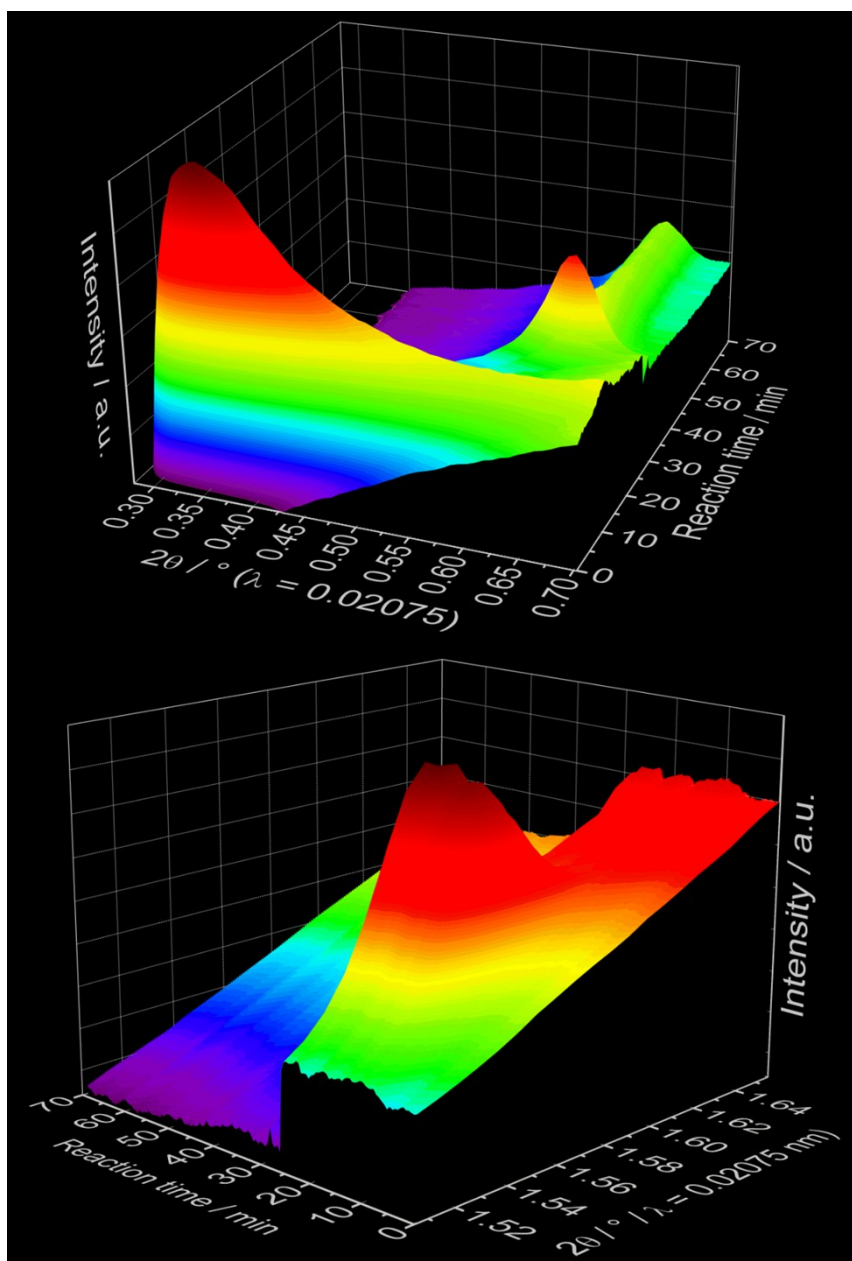


Figure S21. *In-situ* XRD measurements carried out at the DESY P02.1 beamline ($\lambda = 0.2075 \text{ \AA}$, 60 keV), showing the time dependence of the XRD signals assigned to the amorphous phase ^[13] at $0.3643^\circ 2\theta$ and $\text{Ca}_8\text{H}_2(\text{PO}_4)_6 \cdot 5\text{H}_2\text{O}$ ^[11] at $0.6347^\circ 2\theta$ (top) as well as assigned to the $\text{CaHPO}_4 \cdot 2\text{H}_2\text{O}$ ^[10] phase at $1.5661^\circ 2\theta$ (bottom) (experiment **10**, Table 1).

8. References

- [1] H. Pan, S. Jiang, T. Zhang and R. Tang, *Methods Enzymol.*, 2013, **532**, 129.
- [2] M. Köppen, unpublished results.
- [3] H. Terraschke, L. R. Arana, P. Lindenberg and W. Bensch, *Analyst*, 2016, **141**, 2588.
- [4] O. H. Seeck, C. Deiter, K. Pflaum, F. Bertam, A. Beerlink, H. Franz, J. Horbach, H. Schulte-Schrepping, B. M. Murphy, M. Greve and O. Magnussen, *J. Synchrotron Radiat.*, 2012, **19**, 30.
- [5] A.-C. Dippel, H.-P. Liermann, J. T. Delitz, P. Walter, H. Schulte-Schrepping, O. Seeck and H. Franz, *J. Synchrotron Radiat.*, 2015, **22**, 675.
- [6] N. Heidenreich, U. Rütt, M. Köppen, A. K. Inge, A.-C. Dippel, R. Suren and N. Stock, manuscript in preparation.
- [7] A. P. Hammersley, ESRF Internal Report, ESRF97HA02T, "FIT2D: An Introduction and Overview", 1997.
- [8] N. Pienack, L. Ruiz Arana, W. Bensch and H. Terraschke, *Crystals*, 2016, **6**, 157/1.
- [9] M. I. Kay, R. A. Young and A. S. Posner, *Nature*, 1964, **204**, 1050.
- [10] C. A. Beevers, *Acta Cryst.*, 1958, **11**, 273.
- [11] W. E. Brown, *Nature*, 1962, **196**, 1048.
- [12] G. MacLennan and C. A. Beevers, *Acta Cryst.*, 1955, **8**, 579.
- [13] M. Wendt, L. K. Mahnke, N. Heidenreich and W. Bensch, *Eur. J. Inorg. Chem.*, 2016, 5393.